BOUNDS ON NUCLEAR MATTER EQUATION OF STATE USING GRAVITATIONAL WAVE AND X-RAY OBSERVATIONS

Josef Zimmerman,[1] Andrew W. Steiner,[2, 3] and Kent Yagi[1]

[1] *Department of Physics, University of Virginia, Charlottesville, Virginia 22904, USA*
[2] *Department of Physics and Astronomy, University of Tennessee, Knoxville, TN 37996, USA*
[3] *Physics Division, Oak Ridge National Laboratory, Oak Ridge, TN 37831, USA*

(Dated: April 2021)

The nuclear equation of state (EoS) is poorly constrained at present. Properties of neutron stars (NSs) such as radius and tidal deformability are strongly correlated with the EoS, providing an opportunity to study nuclear matter through observations of NSs. We constuct a population of EoSs by randomly sampling a multidimensional Taylor expansion, then constructing correlation distributions between the nuclear parameter $K_{\mathrm{sym},0}$, radius R, and tidal deformability Λ. Using NICER measurements of R from PSR J0030+0451 and LIGO measurements of Λ from GW170817, we develop a statistical method to place bounds on $K_{\mathrm{sym},0}$. Work is ongoing to refine the statistical procedures to produce reliable bounds on $K_{\mathrm{sym},0}$.

INTRODUCTION

The supranuclear equation of state (EoS), found in heavy ion collisions [1, 2] and neutron stars (NSs) [3], remains one of the biggest mysteries in nuclear physics and astrophysics to date. Macroscopic properties of an NS, such as radius and tidal deformability, are strongly dependent on the EoS relationship between energy density and pressure. This presents the opportunity to constrain the EoS using multple measurements of independent NS observables, such as x-ray measurements of the NS mass and radius [4–8].

The historic gravitational wave (GW) detection of the merging NS binary system GW170817 [9] by the LIGO/Virgo Collaboration (LVC) presented the first opportunity to probe the interior properties of a NS through the tidal effects on the gravitational waveform [10–17]. During the inspiral, the tidal fields of each NS in the binary system induce a tidal response in the other. This effect is quantified by the *tidal deformability* parameter [18].

More recently, the Neutron Star Interior Composition Explorer (NICER), an X-ray telescope mounted on the International Space Station, performed a direction observation of the mass and radius of PSR J0030+0451 [19–24]. Using these results, many analyses have been performed to place constraints on the EoS [24–27].

In this paper, we utilize a population of parameterized EoSs to quantify the relationship between the EoS, tidal deformability, and radius of a NS. We ultimately construct a statistical method and attempt to place bounds on the EoS utilizing the GW measurements of GW170817 and NICER measurement of J0030. This is an extension of the author's previous work placing bounds on the EoS utilizing only GW170817 [28].

NUCLEAR MATTER PARAMETERS AND EQUATIONS OF STATE

In order to quantify properties of the EoS, we construct EoSs as a parameterized Taylor expansion, allowing correlations between nuclear parameters and NS observables to be extracted. We express the energy per nucleon $e(n,\delta)$ of supranuclear matter as a Taylor expansion in the nucleon number density n and isospin symmetry parameter $\delta \equiv (n_n - n_p)/n$ representing how neutron-richness of the matter, with n_p and n_n as the proton and neutron number densities, respectively.

The expansion goes as follows [28]. We first express $e(n,\delta)$ as the sum of the symmetric matter part $e(n,0)$ plus the leading asymmetric part $S_2(n)$ as

$$e(n,\delta) = e(n,0) + S_2(n)\delta^2 + \mathcal{O}(\delta^4). \tag{1}$$

We can further expand the symmetric part about nuclear saturation density n_0 using the parameters as

$$e(n,0) = e_0 + \frac{K_0}{2}y^2 + \frac{Q_0}{6}y^3 + \mathcal{O}(y^4), \tag{2}$$

where $y \equiv (n - n_0)/3n_0$ and the coefficients represent energy per nucleon e_0, incompressibility K_0, and third derivative term Q_0, respectively. Similarly, we can expand the asymmetric part as

$$S_2(n) = J_0 + L_0 y + \frac{K_{\mathrm{sym},0}}{2}y^2 + \mathcal{O}(y^3), \tag{3}$$

where the coefficients represent symmetry energy J_0, its slope L_0, and its curvature $K_{\mathrm{sym},0}$. The lower order parameters in the expansion, such as J_0 and L_0, have been constrained with nuclear experiments [29]. On the other hand, neutron star observations can be used to measure higher order parameters like $K_{\mathrm{sym},0}$ due to their large central densities. In this paper, we exclusively focus on placing bounds on $K_{\mathrm{sym},0}$ by combining results from GW170817 and the recent NICER measurements of the neutron star radius. Throughout this paper, we adopt the convention $G = c = 1$.

In order to maintain a model-agnostic approach and minimize systematic biases from the assumptions of EoSs motivated by microscopic physical models, we consider only EoS generated using the form of Eqs. (1)-(3). EoSs were created by randomly sampling each nuclear parameter from a uniform prior, then running tests of the physical properties of the nuclear matter and corresponding NS properties. We required that EoSs must maintain an increasing pressure p with respect to energy density ϵ as $\frac{\mathrm{d}p}{\mathrm{d}\epsilon} > 0$. Additionally, we require the speed of sound $c_s = \sqrt{\frac{\partial p}{\partial \epsilon}} < c$ to remain causal at any central pressure p_0 below the maximum mass defined by $\frac{\partial M}{\partial p_0}|_{M_{max}} < 0$. Additionally, we rejected EoSs inconsistent with the 90% confidence bounds on L_0 and J_0 described in [29]. Lastly, we require that all EoSs support NSs with $M_{max} > 1.96 M_\odot$ [30]. All the EoS models considered here contain pure nuclear matter and do not contain hyperons, Bose condensates, quarks, or any other phase transition.

MASS, RADIUS AND TIDAL DEFORMABILITY

Using the population of EoSs, we compute observable NS properties, such as the mass-radius relationship and tidal deformability for each. Mass and radius are calculated by solving the Tolman-Oppenheimer-Volkhoff equations for an isolated non-spinning NS. By varying the central pressure as an initial condition, the radius of the NS is determined by the location where pressure vanishes, while mass is extracted by matching the asymptotic behaviour of the gravitational potential to the Newtonian case. Figure 1 shows the distribution of mass-radius curves up to 1.96 $M_\odot$ for the EoS population.

The tidal deformability λ of a NS quantifies its elasticity to develop a quadrupole moment Q_{ij} in the presence of an external tidal field $\mathcal{E}_{ij}$ as

$$Q_{ij} = -\lambda\, \mathcal{E}_{ij}. \tag{4}$$

Q_{ij} and $\mathcal{E}_{ij}$ are both obtained from the asymptotic behavior of the gravitational potential around a tidally-deformed NS. Such a stellar solution can be constructed by perturbing the non-rotating, isolated background solution derived earlier and solving a set of perturbed Einstein equations. [28]. An alternative method can be used to approximate λ using the universal relations between compactness $C \equiv M/R$ and $\Lambda \equiv \lambda/M^5$ [31].

$$\Lambda \approx 2.718^{-0.07092(-355+2.236\sqrt{4901+56400C})}. \tag{5}$$

Due to the strong coupling of tidal interaction in a binary system, it is difficult to independently measure Λ_1 and Λ_2 for each NS. Rather, we compute the mass-averaged tidal deformability

$$\tilde{\Lambda} = \frac{16}{13}\frac{(1+12q)\Lambda_1 + (12+q)q^4\Lambda_2}{(1+q)^5}, \tag{6}$$

where $q \equiv m_2/m_1 < 1$ is the mass ratio and m_A and Λ_A represents the mass and dimensionless tidal deformability of the Ath neutron star respectively.

EXTRACTING CORRELATIONS

With a large population of EoSs generated and observables calculated, the next step is to construct distributions relating each relevant property of the EoS.

We begin by clarifying the role of mass in these relationships. Each nuclear parameter is determined only by the fundamental microscopic interactions of nucleons, and is thus independent of macroscopic properties of the NS such as mass. Thus, each EoS has a singular value for each parameter, including $K_{\mathrm{sym},0}$. The NS radius, as shown in Fig 1, can vary significantly with mass. We notate the radius R associated with a particular mass M as R_m. Lastly, while Λ does vary with mass primarily due to the associated variation of radius, $\tilde{\Lambda}$ can be considered a qauntity independent of M. Previous work by the authors established that correlations between $K_{\mathrm{sym},0}$ and $\tilde{\Lambda}$ are dominated by the chirp mass

$$\mathcal{M} \equiv \left[\frac{1}{1+q^2}\right]^{3/5}(m_1+m_2), \tag{7}$$

rather than the exact mass ratio itself [28]. Because $\mathcal{M}$ is very well constrained by GW170817, we adopt the mean values of m_1 and m_2 as measured by the LVC and ignore uncertainty in q. Thus, we obtain a singular value of $\tilde{\Lambda}_{1.186}$ predicted by each EoS that should have been observed in GW170817, independent of any mass uncertainty.

Because the population of EoSs provides only discrete points, we must interpolate to produce a continuous distribution. We use binning and interpolation to produce a continuous distribution $P(K_{\mathrm{sym},0}, R_m, \tilde{\Lambda}_{1.186})$ between R_m, $\tilde{\Lambda}_{1.186}$ and $K_{\mathrm{sym},0}$, rather than assuming a Gaussian relationship as in previous work. [28].

Finally, we must normalize the relationships as conditional probability distributions on R_m and $\tilde{\Lambda}_{1.186}$, performed as

$$P(K_{\mathrm{sym},0}|R_m,\tilde{\Lambda}_{1.186}) = \frac{P(K_{\mathrm{sym},0}, R_m, \tilde{\Lambda}_{1.186})}{\int_{-\infty}^{\infty} P(K'_{\mathrm{sym},0}, R_m, \tilde{\Lambda}_{1.186})\mathrm{d}K'_{\mathrm{sym},0}}. \tag{8}$$

BOUNDS ON $K_{\mathrm{sym},0}$ FROM NICER

We now describe the process to derive bounds on $K_{\mathrm{sym},0}$ from the NICER's measurement of the NS mass

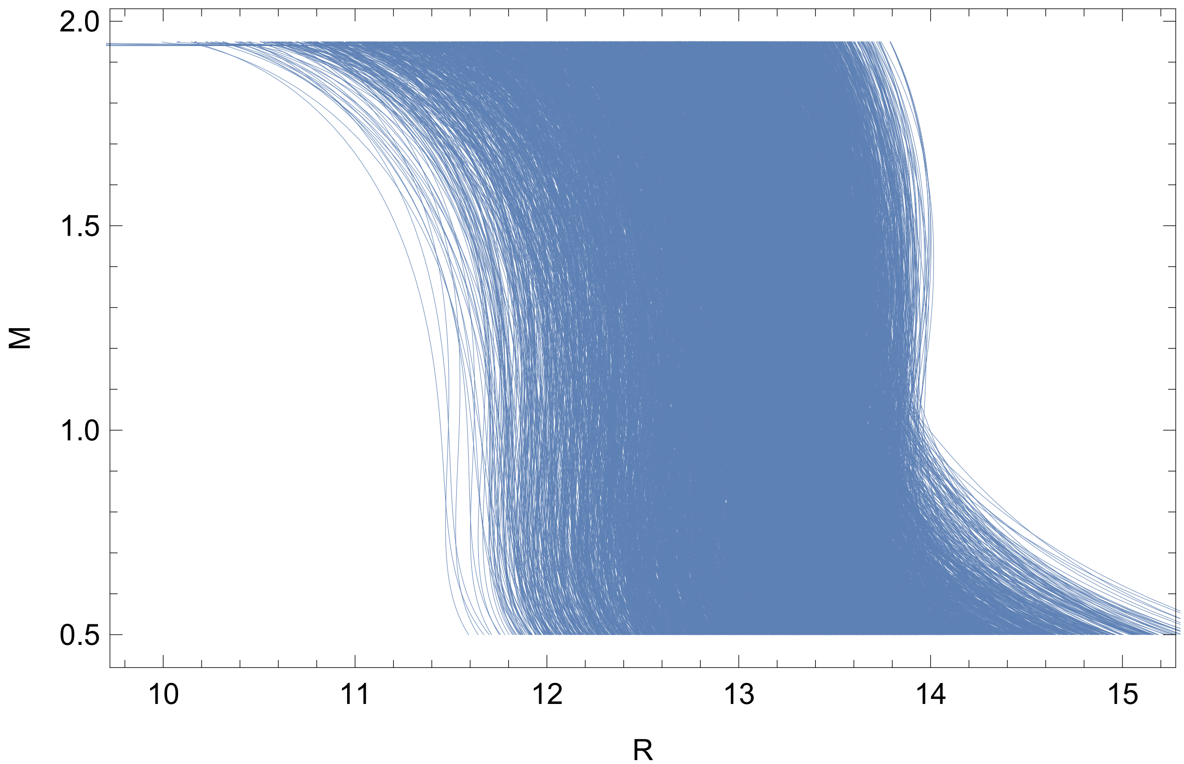

FIG. 1. Relations between the NS mass ($M_{\odot}$) and radius (km) for the population of EoSs.

and radius for PSR J0030+0451. We explore the results of the NICER study [20], released as the Monte Carlo Markov Chain (MCMC) samples for pairs of mass and radius measured from the NS. Because of the strong degeneracy between mass and radius in the NICER posterior measurement, our statistical procedures must account for uncertainty in mass. We accomplish this by constructing bins of nearly constant mass from the NICER posterior. This is performed such that the statistical uncertainty of radius R_m samples falling within that bin is much greater than the difference in average radius measurement between different mass bins $\Delta\overline{R}_m \equiv \overline{R}_{(m+\delta)} - \overline{R}_m$. We first divide NICER's results into 20 bins of mass evenly spaced between 1 and 1.95 $M_{\odot}$[1]. The MCMC samples within each mass bin that starts with mass M give us the probability distribution of the radius samples at that fixed mass M. The samples of R that fall within the bin allow us to construct one-dimensional posterior approximations for $P(R_m)$, which are shown in Fig 2 to reconstruct the entire distribution by Miller et al. [20].

By converting the J0030 measurements into a series of measurements binned by nearly definite mass, we match the conditional probability distributions obtained from the EoS population, which only permit a measurement

[1] We have checked that when we increase the number of bins to 40, the final bound on $K_{\mathrm{sym},0}$ only changed by less than 1 MeV.

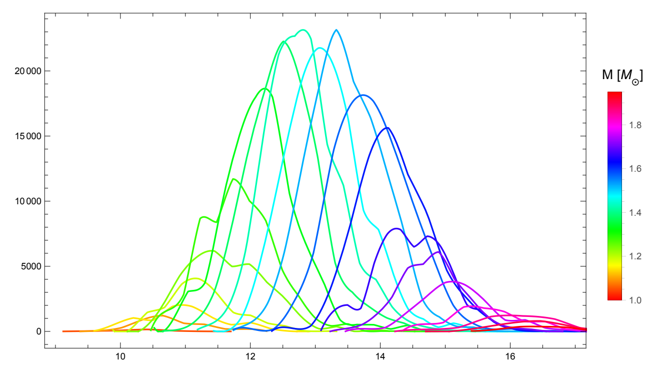

FIG. 2. 20 mass bins, each with a width of 0.05 $M_{\odot}$ divide the NICER measurement into approximations for $P(R_m)$ with small uncertainty in m relative to the statistical spread of R_m. Added together, the 20 distributions for $P(R_m)$ reconstruct the original NICER measurement by Miller et al.[20]

of radius given a definite mass, rather than a correlated uncertainty between the two quantities. One such distribution is shown in Fig 3, which suggests that more positive values of $K_{\mathrm{sym},0}$ are consistent with the data. Additionally, part of the distribution for $P(R_m)$ extends beyond the range of radii observed in the simulated EoS population, indicating that our population may be inconsistent with the NICER measurements.

The final step is to attempt to place probabilistic

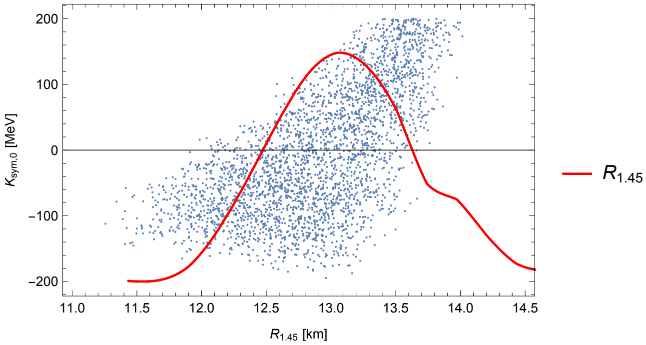

FIG. 3. A single mass bin for $R_1.45$ is shown, with the scatterplot distribution for $P(K_{\text{sym},0}, R_1.45)$ and the NICER measurement for $P(R_1.45)$. The distributions favor more positive values of $K_{\text{sym},0}$, and even extend to slightly larger radii than were consistent with the results from EoS population synthesis.

bounds on $K_{\text{sym},0}$ using a combination of the observed data and simulated correlations, which is achieved using marginalization integrals. Using only the NICER X-ray measurements, the probability distribution of $K_{\text{sym},0}$ from one mass bin at M is given by

$$P_{\text{M}}(K_{\text{sym},0}) = \int_{-\infty}^{\infty} P_{\text{M}}(K_{\text{sym},0}|R_{\text{M}})\, P(R_{\text{M}})\, dR_{\text{M}}. \quad (9)$$

where $P_{\text{M}}(K_{\text{sym},0}|R_{\text{M}})$ is the two-dimensional conditional probability distribution corresponding to Eq. (8). This way, we can take into account the amount of scattering in the correlation between $K_{\text{sym},0}$ and R_{M}, which adds a systematic error to the final distribution on $K_{\text{sym},0}$. After normalizing it properly, this yields bounds on $K_{\text{sym},0}$ for each fixed value of mass M. The final step combines each bound weighted by the probability distribution of the mass $P(M)$ constructed from the number of NICER samples in each mass bin:

$$P(K_{\text{sym},0}) = \sum P_{\text{M}}(K_{\text{sym},0}) P(M). \quad (10)$$

Due to the misalignment between $P(R_m)$ and $P_m(K\text{sym}, 0, R_m)$, the marginalization calculation does not yield reasonable bounds. The final bounds on $K_{\text{sym},0}$ are constrained by the prior uniform sampling limit of $K_{\text{sym},0} < 200$ MeV. For example, previous bounds of $K_{\text{sym},0} = -125 \pm 79$ MeV [32] and $K_{\text{sym},0} = -230^{+90}_{-50}$ MeV [33] are both constrained well below our 200 MeV limit. Even accounting for differences in assumptions, this inconsistency is not explainable statistically.

One possible resolution to the inconsistent bounds on $K_{\text{sym},0}$ may be to include a secondary constraint from the LVC measurement of GW170817. Because the NICER measurement favors larger values of $K_{\text{sym},0}$, the GW170817 measurement's realtively negative bounds on $K_{\text{sym},0}$ may taper the outlying probabilities [28].

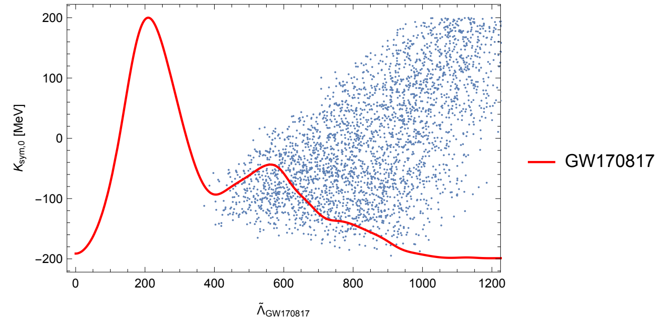

FIG. 4. The LVC measurement of $\tilde{\Lambda}$ for GW170817 is inconsistent with the population of EoSs, which do not display values below 400. This is almost certainly due to an error in the current analysis.

We use the three-dimensional probability distribution $P_{\text{M}}(K_{\text{sym},0}|R_{\text{M}}, \tilde{\Lambda}_{1.186})$ from Eq. (8) relating $K_{\text{sym},0}$, R_{M} and $\tilde{\Lambda}_{1.186}$. We can first use the tidal measurement of $P(\tilde{\Lambda}_{1.186})$ by the LVC [34] to marginalize the above three-dimensional probability distribution over $\tilde{\Lambda}_{1.186}$ to obtain $P_{\text{M}}(K_{\text{sym},0}, R_{\text{M}})$:

$$P_{\text{M}}(K_{\text{sym},0}|R_{\text{M}}) = \int_{-\infty}^{\infty} P_{\text{M}}(K_{\text{sym},0}|R_{\text{M}}, \tilde{\Lambda}_{1.186}) \times P(\tilde{\Lambda}_{1.186})\, \mathrm{d}\tilde{\Lambda}_{1.186}. \quad (11)$$

We then proceed according to Eqs. (9) and (10) to obtain final bounds on $K_{\text{sym},0}$. Research is ongoing to compute this statistical bound using numerical methods properly and ensure that the final bounds are statistically reasonable. The presently calculated distribution between $K_{\text{sym},0}$ and $\tilde{\Lambda}_{1.186}$, shown in Fig 6 also appears inconsistent with the measurement of GW170817 in the small $K_{\text{sym},0}$ region. This finding is inconsistent with the past investigation of $\tilde{\Lambda}$ and $K_{\text{sym},0}$ using randomly sampled EoSs, indicating an error in our present analysis [28].

CONCLUSIONS AND DISCUSSIONS

We constructed a large population of randomly sampled Taylor expanded EoSs, quantifying the relationships between the nuclear parameter $K_{\text{sym},0}$ and the physical observables R and $\tilde{\Lambda}$. By constructing multidimensional conditional probability distributions, we designed a statistical process that can place bounds on $K_{\text{sym},0}$ given a measurement of radius and tidal deformability of a NS. While complications have prevented reliable boudns on $K_{\text{sym},0}$ from being obtained thus far, work is continuing to produce reasonable constraints on the EoS.

Future work includes the possibility of modeling higher order Taylor expansion parameters such as $J_{\text{sym},0}$, the 3rd order symmetry coefficient, which may change the bounds on $K_{\text{sym},0}$ and alleviate some of the inconsistency issues currently faced. In addition, new observables such as the NS moment of inertia can by studied using hypothetical data sets to determine how well $K_{\mathrm{sym},0}$ can be constrained by future observations.

Acknowledgments— J.Z. was supported by the Virginia Space Grant Consortium.

---

[1] P. Danielewicz, R. Lacey, and W. G. Lynch, Science **298**, 1592 (2002), arXiv:nucl-th/0208016 [nucl-th].

[2] M. Tsang, Y. Zhang, P. Danielewicz, M. Famiano, Z. Li, W. Lynch, and A. Steiner, Phys.Rev.Lett. **102**, 122701 (2009), arXiv:0811.3107 [nucl-ex].

[3] J. Lattimer and M. Prakash, Astrophys.J. **550**, 426 (2001), arXiv:astro-ph/0002232.

[4] T. Guver and F. Ozel, Astrophys. J. **765**, L1 (2013), arXiv:1301.0831 [astro-ph.HE].

[5] F. Ozel, G. Baym, and T. Guver, Phys.Rev. **D82**, 101301 (2010), arXiv:1002.3153 [astro-ph.HE].

[6] A. W. Steiner, J. M. Lattimer, and E. F. Brown, Astrophys.J. **722**, 33 (2010).

[7] J. M. Lattimer and A. W. Steiner, The European Physical Journal A **50** (2014), 10.1140/epja/i2014-14040-y.

[8] F. Ozel and P. Freire, Ann. Rev. Astron. Astrophys. **54**, 401 (2016), arXiv:1603.02698 [astro-ph.HE].

[9] B. P. Abbott *et al.* (Virgo, LIGO Scientific), Phys. Rev. Lett. **119**, 161101 (2017), arXiv:1710.05832 [gr-qc].

[10] B. P. Abbott *et al.* (LIGO Scientific, Virgo), Phys. Rev. **X9**, 011001 (2019), arXiv:1805.11579 [gr-qc].

[11] B. P. Abbott *et al.* (LIGO Scientific, Virgo), Phys. Rev. Lett. **121**, 161101 (2018), arXiv:1805.11581 [gr-qc].

[12] V. Paschalidis, K. Yagi, D. Alvarez-Castillo, D. B. Blaschke, and A. Sedrakian, Physical Review D **97** (2018), 10.1103/physrevd.97.084038.

[13] G. F. Burgio, A. Drago, G. Pagliara, H. J. Schulze, and J. B. Wei, Arxiv (2018), 1803.09696v1.

[14] T. Malik, N. Alam, M. Fortin, C. Providência, B. K. Agrawal, T. K. Jha, B. Kumar, and S. K. Patra, Phys. Rev. **C98**, 035804 (2018), arXiv:1805.11963 [nucl-th].

[15] P. Landry and R. Essick, Phys. Rev. **D99**, 084049 (2019), arXiv:1811.12529 [gr-qc].

[16] L. Baiotti, Prog. Part. Nucl. Phys. **109**, 103714 (2019), arXiv:1907.08534 [astro-ph.HE].

[17] A. Guerra Chaves and T. Hinderer, J. Phys. **G46**, 123002 (2019), arXiv:1912.01461 [nucl-th].

[18] É. É. Flanagan and T. Hinderer, Physical Review D **77** (2008), 10.1103/physrevd.77.021502.

[19] T. E. Riley, A. L. Watts, S. Bogdanov, P. S. Ray, R. M. Ludlam, S. Guillot, Z. Arzoumanian, C. L. Baker, A. V. Bilous, D. Chakrabarty, K. C. Gendreau, A. K. Harding, W. C. G. Ho, J. M. Lattimer, S. M. Morsink, and T. E. Strohmayer, The Astrophysical Journal **887**, L21 (2019).

[20] M. C. Miller, F. K. Lamb, A. J. Dittmann, S. Bogdanov, Z. Arzoumanian, K. C. Gendreau, S. Guillot, A. K. Harding, W. C. G. Ho, J. M. Lattimer, R. M. Ludlam, S. Mahmoodifar, S. M. Morsink, P. S. Ray, T. E. Strohmayer, K. S. Wood, T. Enoto, R. Foster, T. Okajima, G. Prigozhin, and Y. Soong, The Astrophysical Journal **887**, L24 (2019).

[21] S. Bogdanov, S. Guillot, P. S. Ray, M. T. Wolff, D. Chakrabarty, W. C. G. Ho, M. Kerr, F. K. Lamb, A. Lommen, R. M. Ludlam, R. Milburn, S. Montano, M. C. Miller, M. Bauböck, F. Özel, D. Psaltis, R. A. Remillard, T. E. Riley, J. F. Steiner, T. E. Strohmayer, A. L. Watts, K. S. Wood, J. Zeldes, T. Enoto, T. Okajima, J. W. Kellogg, C. Baker, C. B. Markwardt, Z. Arzoumanian, and K. C. Gendreau, The Astrophysical Journal **887**, L25 (2019).

[22] S. Bogdanov, F. K. Lamb, S. Mahmoodifar, M. C. Miller, S. M. Morsink, T. E. Riley, T. E. Strohmayer, A. K. Tung, A. L. Watts, A. J. Dittmann, D. Chakrabarty, S. Guillot, Z. Arzoumanian, and K. C. Gendreau, The Astrophysical Journal **887**, L26 (2019).

[23] S. Guillot, M. Kerr, P. S. Ray, S. Bogdanov, S. Ransom, J. S. Deneva, Z. Arzoumanian, P. Bult, D. Chakrabarty, K. C. Gendreau, W. C. G. Ho, G. K. Jaisawal, C. Malacaria, M. C. Miller, T. E. Strohmayer, M. T. Wolff, K. S. Wood, N. A. Webb, L. Guillemot, I. Cognard, and G. Theureau, The Astrophysical Journal **887**, L27 (2019).

[24] G. Raaijmakers, T. E. Riley, A. L. Watts, S. K. Greif, S. M. Morsink, K. Hebeler, A. Schwenk, T. Hinderer, S. Nissanke, S. Guillot, Z. Arzoumanian, S. Bogdanov, D. Chakrabarty, K. C. Gendreau, W. C. G. Ho, J. M. Lattimer, R. M. Ludlam, and M. T. Wolff, The Astrophysical Journal **887**, L22 (2019).

[25] J.-E. Christian and J. Schaffner-Bielich, (2019), arXiv:1912.09809 [astro-ph.HE].

[26] J.-L. Jiang, S.-P. Tang, Y.-Z. Wang, Y.-Z. Fan, and D.-M. Wei, (2019), arXiv:1912.07467 [astro-ph.HE].

[27] G. Raaijmakers *et al.*, (2019), arXiv:1912.11031 [astro-ph.HE].

[28] Z. Carson, A. W. Steiner, and K. Yagi, Phys. Rev. D **99**, 043010 (2019).

[29] I. Tews, J. M. Lattimer, A. Ohnishi, and E. E. Kolomeitsev, The Astrophysical Journal **848**, 105 (2017).

[30] H. T. Cromartie *et al.*, Nat. Astron. **4**, 72 (2019), arXiv:1904.06759 [astro-ph.HE].

[31] K. Yagi and N. Yunes, Phys. Rept. **681**, 1 (2017), arXiv:1608.02582 [gr-qc].

[32] J. Dong, W. Zuo, J. Gu, and U. Lombardo, Phys. Rev. C **85**, 034308 (2012).

[33] W.-J. Xie and B.-A. Li, Astrophys. J. **883**, 174 (2019), arXiv:1907.10741 [astro-ph.HE].

[34] B. P. Abbott *et al.* (LIGO Scientific, Virgo), Phys. Rev. Lett. **121**, 161101 (2018), arXiv:1805.11581 [gr-qc].